Translation of nanomedicines from lab to industrial scale synthesis: The case of squalene-adenosine nanoparticles

Flavio Dormont, Marie Rouquette, Clement Mahatsekake, Frédéric Gobeaux, Arnaud Peramo, Romain Brusini, Serge Calet, Fabienne Testard, Sinda Lepetre-Mouelhi, Didier Desmaele, et al.

Translation of Nanomedicines from Lab to Industrial Scale Synthesis: The Case of Squalene-Adenosine Nanoparticles

Flavio Dormont[a], Marie Rouquette[a], Clement Mahatsekake[b], Frédéric Gobeaux[c], Arnaud Peramo[a] Romain Brusini[a], Serge Calet[b], Fabienne Testard[c], Sinda Lepetre-Mouelhi[a], Didier Desmaële[a], Mariana Varna[a], Patrick Couvreur[a]

[a] *Institut Galien Paris-Sud, CNRS UMR 8612, Université Paris-Sud, Université Paris-Saclay, 92296 Châtenay-Malabry, France*

[b] *HOLOCHEM, Voie de l'Innovation, 27100 Val-de-Reuil, France*

[c] *CEA Saclay, CNRS UMR 3685, Université Paris-Saclay, 91191 Gif sur Yvette, France*

Corresponding author: Patrick Couvreur

Email: patrick.couvreur@u-psud.fr
Tél: +33 146 835 582 (secretariat)
+33 146 835 396 (direct)
Fax: +33 146 619 334

ABSTRACT

A large variety of nanoparticle-based delivery systems have become increasingly important for diagnostic and/or therapeutic applications. Yet, the numerous physical and chemical parameters that influence both the biological and colloidal properties of nanoparticles remain poorly understood. This complicates the ability to reliably produce and deliver well-defined nanocarriers which often leads to inconsistencies, conflicts in the published literature and, ultimately, poor translation to the clinics. A critical issue lies in the challenge of scaling-up nanomaterial synthesis and formulation from the lab to industrial scale while maintaining control over their diverse properties. Studying these phenomena early on in the development of a therapeutic agent often requires partnerships between the public and private sectors which are hard to establish.

In this study, through the particular case of squalene-adenosine nanoparticles, we reported on the challenges encountered in the process of scaling-up nanomedicines synthesis. Here, squalene (the carrier) was functionalized and conjugated to adenosine (the active drug moiety) at an industrial scale in order to obtain large quantities of biocompatible and biodegradable nanoparticles. After assessing nanoparticle batch-to-batch consistency, we demonstrated that the presence of squalene analogs resulting from industrial scale-up may influence several features such as size, surface charge, protein adsorption, cytotoxicity and crystal structure. These analogs were isolated, characterized by multiple stage mass spectrometry, and their influence on nanoparticle properties further evaluated. We showed that slight variations in the chemical profile of the nanocarrier's constitutive material can have a tremendous impact on the reproducibility of nanoparticle properties. In a context where several generics of approved nanoformulated drugs are set to enter the market in the coming years, characterizing and solving these issues is an important step in the pharmaceutical development of nanomedicines.

Keywords: squalene-adenosine nanoparticles, drug development, impurity profile, scaling-up nanomedicines

1. INTRODUCTION

Nanostructured drug delivery systems have emerged over the last several decades as an important field of academic research and are set to bring momentous advances to human health through clinical and industrial developments. While a first generation of nanocarriers were successfully brought to market, notably in the oncology field, new classes of therapeutic agents making use of polymers, proteins, nucleic acids and other biomolecules have emerged for the treatment of numerous diseases[1,2]. Unfortunately, these new types of nanocarriers are facing difficulties in their translation to the clinics due to an absence of realistic industrial production, lack of reproducibility and insufficient cost-effectiveness[3]. Part of the problem lies in the fact that nanostructured drug delivery systems have grown into increasingly complex structures with poorly understood biological fates[4]. Size[5], surface charge[6], morphology[7], drug release profiles[8] and interaction with blood components[9] have all been shown to be key parameters that influence the biomedical outcome of nanocarriers *in vivo***.** Controlling these numerous parameters in a reproducible manner over intricate structures can be problematic, as well as difficult to bring to industrial standards. Accordingly, recent studies have highlighted the importance of developing simple and robust manufacturing methods that ensure the proper formulation of nanomaterials in large scales[10,11].

Another critical issue lies in the challenge of scaling-up the synthesis of a nanocarrier's constitutive materials. Guidelines from the pharmaceutical industry in terms of good manufacturing practice and pharmaceutical quality can be applied, but the nature and complexity of nanomaterials carry their extra set of challenges. Indeed, while any scale-up of laboratory processes is difficult, nanomaterials production is made more challenging by the fact that subtle variations in the synthesis and manufacturing processes can result in significantly different products. The matter is further complicated when one considers that carriers (*e.g.* polymers, lipids, dendrimers) often inherently do not have a single pharmaceutical identity, but are constituted of a raft of different molecules which are difficult to individually characterize. This is contrary to conventional small-drug therapeutics, where the active pharmaceutical ingredient is the main concern. While regulations are still unclear regarding the plural identity of nanomedicines, special care should be taken when considering production of nanomaterials. Namely, there must be robust quality control systems in place, validating batch-to-

batch consistency and biological equivalence. Identifying critical parameters that might affect the reproducibility of nanomaterial properties early on and monitoring these parameters on multiple batches is a good practice which can minimize the appearance of reproducibility issues later on[12].

Recently, squalenoylation (i.e squalene loaded with active molecules) has emerged as a simple, safe and efficient method to produce nanoparticles encapsulating a vast range of therapeutic agents[13-15]. Conjugating squalene, an endogenous, biocompatible and biodegradable lipid to a drug candidate yields nanocarriers with high drug loading efficiency, low toxicity, and high blood residence time[16]. These nanoparticles have been used in pre-clinical models to treat a host of afflictions from cancer[17] to ischemic stroke[18] and pain[19]. As with other nanomedicines, efforts now need to focus on the translation from lab-scale experiments to semi-industrial batches, allowing eventual regulatory approval for clinical trials.

In this article, through the example of squalene-adenosine (SQAd) nanoparticles, we wish to report on the challenges encountered in the process of scaling-up nanomaterial synthesis by comparing two batches, one synthesized at the gram scale, the other at the kilogram scale by an industrial partner. We highlight specific parameters which needed to be closely monitored to ensure batch-to-batch consistency. Notably, we demonstrate that scaling of lab scale synthetic processes can induce varying impurity profiles which can have tremendous impact on the reproducibility of the biological and physicochemical properties of nanoparticle from batch-to-batch.

2. MATERIALS AND METHODS

2.1. Materials.

Squalene, adenosine, N-Bromosuccinimide (NBS), 1-hydroxybenzotriazole hydrate HOBt, 2-(1H-7-azabenzotriazol-1-yl)-1,1,3,3-tetramethyluronium hexafluorophosphate (HATU),, tetrabutylammonium fluoride (TBAF), aluminium isopropoxide, propionic acid, triethyl orthoacetate, triethylamine (NEt_3), diisopropylethylamine (DIPEA), formic acid, 3-(4,5-dimethylthiazol-2-yl)-2,5-diphenyltetrazolium bromide (MTT), penicillinstreptomycin solution, glutamine, norepinephrine, Claycomb's Medium, Dulbecco's Modifidied Eagle's Medium (DMEM) and dextrose (DXT) were purchased from Sigma-

Aldrich (France). Ultra-pure water was prepared using a MilliQ system (Millipore Corporation, Billerica, MA). Reagents and HPLC grade solvents as ethanol, methanol, ethyl acetate, and acetonitrile were provided by Carlo Erba (France). Ammonium acetate $CH_3CO_2NH_4$ was from VWR

2.2.1. Synthesis of 3-bromo-2,6,10,15,19,23-Hexamethyl-tetracosa-6,10,14,18,22-pentaen-2-ol (squalene bromohydrine) **2.**

To a stirred solution of squalene **1** (1000 g, 2.4 mol) in THF (5 L), H_2O (200 mL) was slowly added until the solution became opalescent. To this mixture, THF (100 mL) was slowly introduced until solution became clear again. N-Bromosuccinimide (520 g, 2.9 mol) was then added and the reaction mixture was stirred 90 min at room temperature after which THF was removed and a liquid-liquid extraction was performed with 500 mL of brine and 1000 mL of diethyl ether. The organic phase was separated and the aqueous phase extracted with diethyl ether (3 x 800 mL). All the organic layers were combined, dried over $MgSO_4$, filtered and concentrated under reduced pressure. The resulting oily residue was purified by flash chromatography over silica gel (cyclohexane/ethyl acetate : 8/1 v/v) to provide bromohydrine **2** (353 g, 29%) as a yellow oil. ^{1}H NMR (300 MHz, $CDCl_3$) δ: 5.25-5.10 (m,5H, *H*C=C(CH_3)), 4.01 (dd, *J* = 2.1, 11.3 Hz, 1H, CHBr), 2.32-2.35 (m, 1H), 1.95-2.19 (m, 18H, CH_2), 1.77-1.88 (m, 1H), 1.70 (s, 3H, CH_3), 1.63 (m, 15H, CH_3), 1.37 (s, 3H, CH_3), 1.36 (s, 3H, CH_3).

2.2.2. Synthesis of 2,3-epoxysqualene-2,2-dimethyl-3,7,12,16,20-pentamethylhenicosa-3,7,11,15,19-pentaen-1-yloxirane (epoxysqualene) **3.**

In a 10 L round bottom flask fitted with a magnetic stirrer and a calcium chloride guard tube, squalene bromohydrine **2** (350 g, 0.69 mol) was solubilized in MeOH (5 L) and K_2CO_3 (2eq) was added to this mixture. The reaction mixture was stirred 2 hours at room temperature and was then concentrated *in vacuo*. The residue was treated with H_2O and extracted with AcOEt (2 x 1 L). The combined organic layers were dried with $MgSO_4$, filtered and the solvent removed under reduced pressure to obtain a yellow oil (280 g, 95%) which was directly used in the next step without any further purification. ^{1}H NMR ($CDCl_3$) δ: 5.25-5.10 (m,5H, *H*C=C(CH_3)), 2.69 (t, *J* = 7.0 Hz, 1H, CH) 1.95-2.19 (m, 20H, CH_2); 1.68 (s, 3H, CH_3) 1.60 (s, 3H, CH_3); 1.58 (m, 12H, CH_3) 1.28 (s, 3H, CH_3); 1.24 (s, 3H, CH_3).

2.2.3. Synthesis of 2,6,10,15,19,23-Hexamethyl-tetracosa-1,6,10,14,18,22-hexaen3-ol 4.

To a stirred solution of 2,3-epoxysqualene **3** (280 g, 0.66 mol) in toluene (2.5 L) was added aluminium isopropoxide (430.8 g, 1.98 mol). The resulting mixture was stirred under reflux for 16 h. After cooling to room temperature, 1 N HCl was added until the whole solid was solubilized. The organic phase was collected and the aqueous phase extracted with diethyl ether (4 x 500 mL). The combined organic layers were washed with brine, dried over $MgSO_4$, filtered and concentrated under reduced pressure. The resulting oily residue was purified by flash chromatographic purification over silica gel (petroleum ether/diethyl ether : 4/1 v/v) to provide allylic alcohol **4** (177.5 g, 63%) as a colourless oil. ^{1}H NMR (300 MHz, $CDCl_3$) δ: 5.25–5.10 (m, 5H, *H*C=C(CH_3)), 4.96 (m, 1H, =C*H*$_2$), 4.86 (m, 1H, =C*H*$_2$), 4.05 (t, *J* = 6.5 Hz, 1H, C*H*OH), 2.20–1.95 (m, 20H, CH_2), 1.75 (s, 3H, CH_3), 1.70 (s, 3H, CH_3), 1.64 (s, 3H, CH_3), 1.63 (s, 12H, CH_3).

2.2.4. Synthesis of 4,8,12,17,21,25-Hexamethyl-hexacosa-4,8,12,16,20,24-hexaenoic acid ethyl ester (squalene acetic ethyl ester) **5.**

A stirred solution of allylic alcohol **4** (175 g, 0.41 mol) and propionic acid (3.5 g, 0.047 mol) in triethyl orthoacetate (1 L) was heated under reflux for 3 h. After cooling to room temperature, triethylamine (7 g, 0.069 mol) was added and the mixture was concentrated under reduced pressure. The residue was stirred for 5 min with 0.1 N HCl solution and extracted with diethyl ether (4 x 500 mL). The combined organic phases were washed with brine, dried over $MgSO_4$, filtered and concentrated under reduced pressure to provide the crude ester **5** (202 g, quantitative) as a pale yellow oil which was directly used in the next step without further purification. ^{1}H NMR (300 MHz $CDCl_3$) δ: 5.20-5.02 (m, 6H, *H*C=C(CH_3)), 4.09 (q, *J* = 7.2 Hz, 2H, OC*H*$_2$$CH_3$), 2.40-2.20 (m, 4H, O_2CC*H*$_2$C*H*$_2$), 2.15-1.85 (m, 20H, CH_2), 1.66 (s, 3H, CH_3), 1.59 (s, 18H, CH_3), 1.23 (t, *J* = 7.2 Hz, 3H, OCH_2C*H*$_3$).

2.2.5 Synthesis of squalenylacetic acid 4,8,12,17,21,25-Hexamethyl-hexacosa-4,8,12,16,20,24-hexaenoic acid (squalenylacetic acid) **6.**

In a 10 L round bottomed flask fitted with a magnetic stirrer, a reflux condenser and a calcium chloride guard tube, was introduced ester **5** (200 g, 0.4 mol) solubilized 3000 mL of EtOH and 1000 mL of THF.

After stirring, $LiOH,H_2O$ (92.5 g, 2.2 mol) was added at room temperature. The mixture was heated to reflux for 24 h. After cooling, the reaction mixture was concentrated under reduced pressure and MilliQ water was added. The mixture was acidified with HCl 3N to pH = 3-4 and was then extracted by MTBE (3 x 1 L). The combined organic extracts were dried over $MgSO_4$, filtered and concentrated under reduced pressure. The residue was purified by flash chromatography on silica gel (Dichloromethane/Petroleum ether : 1/1 (v/v)) to provide squalenylacetic acid **6** (121 g, 65%) as a yellow oil. ^{1}H NMR (300 MHz $CDCl_3$) δ: : 5.15 -5.0 (m, 6H, *H*C=C(CH_3)), 2.49-2.30 (m,4H, $O_2CCH_2CH_2$), 2.20-1.90 (m, 20H, CH_2), 1.70 (s, 3H, CH_3), 1.62 (s, 18H, CH_3).

2.2.6. Synthesis of *N*-{9-3,4-bis[(tert-butyldimethylsilyl)oxy]-5-[(tertbutyldimethylsilyl)oxy] methyloxolan-2-yl]-9H-purin-6-yl}-4,8,12,17,21,25-hexamethylhexacosa-4,8,12,16,20,24-hexaenamide (Tris-O-silylated Squalene Adenosine) **7.**

To a stirred solution of squalenylacetic acid **6** (120 g, 0.25 mol) in anhydrous dichloromethane (1 L) and DMF (5 mL), was added under nitrogen HOBt (46 g, 0.3 mol), HATU (114 g, 0.3 mol), tris-O-silylated adenosine (130.2 g, 0.25 mol) and DIPEA (9.35 g, 0.075 mol). The reaction mixture was stirred 72 hours at room temperature and was then concentrated *in vacuo*. Aqueous sodium hydrogen carbonate was added and the mixture was extracted with ethyl acetate (3 × 500 mL) and dichloromethane (1 × 300 mL). The combined extracts were washed with brine, dried on $MgSO_4$, and concentrated under reduced pressure. The crude product was purified by flash chromatography on silica gel eluting with 10 % ethyl acetate in cyclohexane to give tris-O-silylated Squalene Adenosine **7** as a colourless oil (119 g, 45%); ^{1}H NMR (300 MHz, $CDCl_3$) δ : 8.70 (s,1H, H8), 8.64 (s, 1H NHCO), 8.35 (s, 1H, H2), 6.10 (d, , *J* = 5.2 Hz, 1 H, H1'), 5.20 (t, *J* = 6.4 Hz, 1 H, *H*C=C(CH_3)), 5.20-5.10 (m, 5H, *H*C=C(CH_3)), 4.67 (t, *J* = 4.7 Hz, 1 H, H2'), 4.3 (t, *J* = 4.7 Hz, 1 H, H2'), 4.15-4.11 (m; 1 H, H4'), 4.02 (dd, *J* = 11.2 Hz, *J* = 3.9 Hz, 1H, H5'), 3.78 (dd, *J* = 11.2 Hz, *J* = 2.7 Hz, 1H, H5'), 2.96 (t, *J* = 7.8 Hz, 2 H, $O_2CCH_2CH_2$), 2.45 (t, *J* = 7.8 Hz, 2 H, $O_2CCH_2CH_2$), 2.10-1.95 (m, 20 H, =C(CH_3)CH_2CH_2), 1.67 (s, 6 H, C=C(CH_3)$_2$), 1.58 (s, 15 H, C=C(CH_3)), 0.95 (s, 9 H, *t*-BuSi), 0.93 (s, 9 H, *t*-BuSi), 0.78 (s, 9H, *t*-BuSi), 0.15 (s, 3 H, CH_3Si), 0.14 (s, 3 H, CH_3Si), 0.10 (s, 6H, CH_3Si), −0.04 (s, 3 H, CH_3Si), −0.24 (s, 3 H, CH_3Si).

2.2.7. Synthesis of N-{9-3,4-dihydroxy-5-(hydroxymethyl)oxolan-2-yl]-9H-purin-6-yl}-4,8,12,17,21,25- hexamethylhexacosa-4,8,12,16,20,24-hexaenamide (Squalene-Adenosine) **8.**

To a solution of tris-O-silylated Squalene Adenosine **7** (100 g, 0.94 mol) in dry THF (1 L) was added TBAF (1M solution in THF, 340 mL, 0.34 mol) and the mixture was stirred for 3h at room temperature. The reaction was then quenched with brine and the mixture was extracted with ethyl acetate (3 × 500 mL). The combined extracts were dried on $MgSO_4$, and concentrated under vacuum. The crude product was purified by chromatography on silica gel eluting with 5 % methanol in dichloromethane to give Squalene-Adenosine **8** as a colourless oil (37.1 g, 55 %); ^{1}H NMR (300 MHz, $CDCl_3$) **δ:** 9,39 (broad s, 1 H, N*H*CO), 8.41 (s, 1 H, H8), 8.21 (s, 1 H, H2), 5.98 (d, 1 H, *J* = 5.4 Hz, H1'), 5.32 (t, 1 H, *J* = 6.3 Hz, *H*C=C(CH_3)), 5.05-4.93 (m, 5 H, *H*C=C(CH_3)), 4.61 (t, 1 H, *J* = 4.9 Hz, H2'), 4.18 (m, 1 H, H3'), 3.98 (m, 1 H, H4'), 3.69 (dd, 1 H, *J* = 11.9 Hz, *J* = 3.7 Hz, H5'), 3.57 (dd, *J* = 11.9 Hz, *J* = 3.3 Hz, 1 H, H5'), 2.98 (t, 2 H, *J* = 7.8 Hz, $O_2CCH_2CH_2$), 2.45 (t, 2 H, *J* = 7.8 Hz, $O_2CCH_2CH_2$), 2.11-1.93 (m, 20 H, =C(CH_3)CH_2CH_2), 1.62 (s, 3 H, C=C(CH_3)), 1.60 (s, 3 H, C=C(CH_3)), 1.54 (s, 15 H, C=C(CH_3)).

2.3 Lab scale

synthesis of SQAd (Lab SQAd) SQAd was synthesized as previously reported [18] starting from 20 g of squalene

2.4. HPLC-UV-ESI-MS analysis.

2.4.1. Chromatography Apparatus:

A high-performance liquid chromatograph Waters Alliance 1695 (Waters, Milford, MA), equipped with a Waters DAD 2996 photodiode array detector, Hewlett-Packard computer with a Waters Empower 3 software and a Waters autosampler with a 50 μL loop was used, with simultaneous detection at 220 nm and 270 nm. The spectra (detection wavelengths from 200-600 nm) were recorded for all peaks. The HPLC system was coupled on line with a Waters TOF mass spectrometer.

2.4.2. Columns and Mobile Phase:

A Waters Xselect LC-18 column (2.1 x 150 mm, 3.5 μm) was used. The solvents used were (A) 100% HPLC-grade acetonitrile (B) 0.1% formic acid in MilliQ water. Flow rate: 0.25 mL/min. Solvents and samples were filtered through a 0.45 μm Millipore filter type HA (Millipore Corp., Bedford, MA).

2.4.3. HPLC Conditions:

SQAd and SQAd analogs phase (called Ph1) were separated using a gradient over 10 min from 80% to 100% of A. Peak assignments were made based on spectral data.

2.4.4. Electrospray Mass Spectrometry (ESI-MS).

Mass spectrometry was performed using electrospray MS. The instrument was a Waters TOF LCT Premier mass spectrometer equipped with an ion spray interface with a capillary voltage of 2800 V. The mass spectrometer was operated in the positive-ion mode.

2.5 High Resolution HPLC-ESI-MS^n analysis.

2.5.1. Chromatography Apparatus:

A ThermoFisher Scientific (ThermoFisher, Waltham, MA) chromatograph including a Dionex U-3000 RSLC system equipped with a WPS-3000 autosampler and a TCC-3000 column oven was used. The RSLC system was coupled on-line to a hybrid mass spectrometer LTQ-Orbitrap Velos Pro (ion trap and orbital trap) from ThermoFisher.

2.5.2. Columns and Mobile Phase:

A Macherey-Nagel Nucleodur 100-5 C18 EC column (2.1 x 125 mm) was used. The solvents used were (A) 50% HPLC-grade acetonitrile/ 50% HPLC-grade MeOH (B) 0.1% formic acid in MilliQ water. Flow rate: 0.3 mL/min. Solvents and samples were filtered through a 0.45 μm Millipore filter type HA (Millipore Corp., Bedford, MA).

2.5.3. HPLC Conditions:

SQAd and SQAd analogs were separated using a solvent gradient over 10 min from 80% to 100% of A.

2.5.4. High Resolution Mass Spectrometry: Mass Spectrometry Full Scan analysis was performed in the Orbital Trap with a resolution of 30 000. The instrument was a ThermoFisher hybrid mass spectrometer LTQ-Orbitrap Velos Pro equipped with an ion spray interface with a capillary voltage of 3400 V.

MS^n: MS^n was performed in the LTQ ion trap with Collision Induced Dissociation (CID) at an energy of 35 (arbitrary unit). Fragment detection was performed in the orbitrap with a resolution of 7500.

2.6. Preparative HPLC.

Preparative HPLC separation of Ph1 from SQAd was performed by injecting 1 mL of a filtered solution of 10 mg/mL Ind SQAd sample in ethanol onto a Waters Xselect LC-18 (30 × 150 mm, 2.1 μm) HR C-18 column. Elution was performed using Waters model 501 pumps to deliver a constant flow rate of 42 mL/min. The solvent system used was identical to prior HPLC experiments. SQAd was detected by absorbance at 270 nm using a Waters UV. DAD 2996 photodiode array detector. The first product impurity phase (Ph1) was collected between 13.6 min and 15.3 min and SQAd was collected between 19 min and 21 min.

2.6.1. Peak Extraction.

Fractions of eluates containing compounds of interest were combined, filtered through a 0.22 μm Teflon filter, and concentrated at 50 °C under 0.01 hPa vacuum on a rotary evaporator to obtain purified compound.

2.7. Preparation and Physico-Chemical Characterization of NPs.

SQAd nanoparticles (SQAd NPs) were prepared by nanoprecipitation, as previously described [20,21] (Supplementary Figure S1)**.** Briefly, SQAd was dissolved in absolute ethanol (6 mg/mL) and added dropwise under moderate mechanical stirring to a 5% (w/v) dextrose solution (DXT 5%). The ethanol was then completely evaporated using a Rotavapor (90 rpm, 40 °C, 42 mbar) to obtain an aqueous

suspension of pure NPs (2 mg/mL). Ph1 nanoparticles were obtained from the analog chromatographic fraction using the same protocol. NPs size (hydrodynamic diameter) and surface charge (zeta potential) were measured using a Malvern Zetasizer Nano ZS 6.12 (173° scattering angle, 25 °C, Material RI: 1.49, Dispersant Viscosity RI: 1.330, Viscosity 0.8872 cP). For the size measurements by dynamic light scattering (DLS), a good attenuator value (7−9) was obtained when suspending 50 µL of NPs in 1 mL of distilled water. The mean diameter for each preparation resulted from the average of three measurements of 60 s each. For zeta potential measurements, 70 µL of NPs was dissolved in 2 mL of KCl 1mM before filling the measurement cell. The mean zeta potential for each preparation resulted from the average of three measurements in automatic mode, followed by the application of the Smoluchowski eq. NP stability was assessed by measuring NP size by DLS at different time intervals after initial formulation up to seven days.

2.8. Cryo-Transmission Electron Microscopy (cryo-TEM).

The morphology of SQAd nanoparticles was observed with cryo-transmission electron microscopy. Drops of the solutions were deposited on EM grids covered with a holey carbon film (Quantifoil R2/2) previously treated with a plasma glow discharge. The excess liquid on the grids was blotted out with filter paper, and the grids were quickly immersed in liquid ethane to form a thin vitreous ice film. The whole process was performed using a Vitrobot apparatus (FEI Company). Observations were conducted at low temperature (−180°C) on a JEOL 2010 FEG microscope operated at 200 kV. Images were recorded with a Gatan camera.

2.9. Small-Angle X-ray Scattering

SAXS experiments were performed on two different set-ups. Lab SQAd was studied at the SWAXSLab in CEA Saclay with a Xeuss 2.0 apparatus (Xenocs) equipped with a GeniX3D X-ray generator (λ = 1.542Å) and a PILATUS3 1M 2D detector. The detector to sample distance was chosen to attain the 0.01-0.5 $Å^{-1}$ q-range. Averaging and data treatment were performed with PYSAXS software (https://pypi.org/project/pySAXS/). The sample Ind SQAd was studied at the synchrotron SOLEIL (Saint-Aubin, France) on the SWING beamline. Data were recorded at 12keV with a 4M bi-dimensional Eiger detector in the chosen 0.014-1.9 $Å^{-1}$ q-range. The data treatments were performed using FOXTROT software. For each set-up, the samples were inserted in 1.5 mm diameter quartz capillaries sealed with

paraffin wax and analyzed with a counting time of 3600s and 250 ms for respectively the SWAXSLab and SWING beamlines.

2.10 Spiking experiment.

SQAd and Ph1 were separately dissolved in absolute ethanol (6 mg/mL). The SQAd and Ph1 ethanolic solutions were mixed in varying ratios as to obtain different 0.1 %, 1 %, 5 %, 10 % (w/w) solutions of Ph1 in SQAd. This organic solution was then nanoprecipitated as described above in a 5% (w/v) dextrose solution (Figure 7A).

2.11 Cell Culture.

MCEC (Mouse Cardiac Endothelial Cells, TebuBio, France) cells were grown in DMEM medium supplemented with 10% FBS, 1% penicillin-streptomycin and 1% HEPES at 37 °C and 5% CO2. HL1 (Cardiac Muscle cells, Sigma, France) were grown in Claycomb's medium supplemented with 10% FBS, 1% penicillin-streptomycin, 1% glutamine and 1% norepinephrine at 37 °C and 5% CO2. HepG2 (Hepatocellular Carcinoma, Sigma, France), HUVEC (Human Umbilical Vein Endothelial cell, ATCC, France) and MiaPaca (Human Pancreatic Carcinoma Epithelial Cells, ATCC, France) cells were grown in DMEM medium supplemented with 10% FBS and 1% penicillin-streptomycin at 37 °C and 5% CO2 atmosphere. For HL1 and MCEC cell lines, cells were divided to the tenth every 3-4 days. For MiaPaca, HepG2 and HUVEC cells, cells were divided to the fifth every 3-4 days.

Cytotoxicity of SQAd NPs.

2.12 Cytotoxicity was evaluated using an MTT (3-[4,5-dimethylthiazole-2-yl]-2,5-diphenyltetrazolium bromide) assay. For a typical 24 hours cytotoxicity study, cells were seeded in a 96 well plate at 8000 cells/well (30 000 cells/cm^2) for 24 hours. Subsequently, cells were treated with different concentrations of nanoparticles ranging from 1 μM to 200 μM in 200 μL of complete cell medium. Cells were incubated for 24 hours before the MTT assay was performed. For the MTT assay, cells were washed with PBS, and incubated for 2 hours with medium containing 0.5 mg/mL of MTT. The medium

was removed after 2 hours and 100 μL of DMSO were added to each well before measuring absorbance reading on a Perkin Elmer absorbance reader at 570 nm.

2.13. Rat Plasma Samples.

Rat blood samples were obtained from healthy male Sprague Dawley rats by cardiac puncture and collected into heparinated collection tubes. Plasma was obtained by centrifuging the blood samples at 2000 rcf for 10 min. Plasma samples were pooled, split into 5 mL aliquots and stored at -80 °C until further use. For protein binding experiments, the aliquots were thawed at room temperature and then incubated at 37 °C.

2.14. Protein Assay.

Plasma protein binding to SQAd nanoparticles was studied by incubating 250 μL of NP suspension (4 mg/mL) in DXT 5% with 250 μL of rat plasma. Incubation was carried on at 37 °C for 1 h to promote protein adsorption. The amount of adsorbed proteins on SQAd NPs after incubation in plasma was quantified using the Protein Assay reagent (Pierce, Thermo Scientific, Waltham, MA, USA) according to manufacturer's protocol. Briefly, after incubation, NP-protein complexes were centrifuged at 16000 rcf for 10 min to pellet NP- protein complexes. The supernatant was removed and the pellet was resuspended in 500 μL of PBS. This procedure was repeated twice to remove any loosely bound proteins until final suspension in 500 μL of PBS. A plasma aliquot not incubated with nanoparticles was subjected to the same procedure as control. For the assay, 25 μL of each sample were placed in a 96-well plate and 200 μL of Protein Assay working solution were added. The measures were performed in triplicate. The plate was covered, mixed on an orbital plate shaker, and incubated at 37 °C for 30 min. The absorbance of each sample, standard and blank was measured with a Perkin Elmer absorbance reader at 570 nm. The protein concentration was calculated using interpolation with the standard curve obtained from PBS solutions of Bovine Serum Albumin.

2.15. Protein Separation by 1D-PAGE.

Proteins were separated by 1D-PAGE according to Laemmli[22] with some modifications. Proteins were desorbed from SQAd NPs by adding SDS-PAGE sample buffer to the pellet and heating the solution to 95 °C for 5 min. A Biorad Mini-PROTEAN® TGX Stain-Free™ 4%-15% Bis–Tris polyacrylamide gel was used as separating gel. Electrophoresis was carried out at a constant voltage of 300 V in electrophoresis buffer, until the dye front reached the lower end of the gel (20 min). Separated proteins were imaged using a Biorad ChemiDoc Imaging system and analyzed with Biorad Image Lab software.

3. RESULTS AND DISCUSSION

3.1. Scale-up and Reproducibility of NPs properties.

3.3.1. Synthesis of SQAd

At the onset of this study was a need to scale up the synthesis of the SQAd bioconjugates for use in multi-lab pre-clinical trials evaluating SQAd efficacy in different animal models. Starting from squalene, SQAd was first synthesized at a lab scale in limited amounts (ie. 100 mg) with a total yield of ~2 % (Lab SQAd) and then by an industrial partner in large scale using the same synthetic process (Ind SQAd). SQAd synthesized from industrial batches was obtained in a higher total yield (~5 %) through industrial optimization of the synthesis process. The synthetic route to SQAd **8** is illustrated in Figure 1. Because of its lack of functional groups, conjugation to squalene **1** can only be achieved after functionalization of the squalene aliphatic chain. This functionalization process starts with the selective hydroxybromination of the terminal double bond with NBS in wet THF according to the method of Van Tamelen[23]. The bromohydrine **2** pathway shows a proclivity for the formation of the terminal bromohydrine which has been attributed in part to conformational changes of the squalene chain in a water containing solution. This hypothesis is strongly supported by the numerous observations that most epoxidation reactions performed in apolar organic solvents using peroxy acids or dimethyldioxirane give a mixture of internal epoxidation products[24,25]. The chemoselectivity of NBS/H_2O for the terminal double bond was, however, not perfect and the crude material needs to be thoroughly purified by silica gel chromatography before engaging the bromohydrine in the next step.

Nevertheless, this synthetic path was considered preferable to other oxidative methods as the process didn't require the involvement of toxic reagents or heavy metals which would further complicate regulatory approval. As depicted in Figure 1A, once the crucial terminal functionalization was obtained, 2,3-oxydosqualene was easily derived from the bromohydrine by potassium carbonate treatment (b). The one isoprene-unit homologation was then achieved by sequential aluminium isopropoxide ring opening reaction (c) followed with Claisen-Johnson rearrangement with triethylorthoacetate (d)[26]. After saponification, the obtained squalenyl acetic acid was coupled to 3',4',5'-trisilylated adenosine using HATU/HOBt as coupling agent with moderate yield. After extensive purification, the silyl protecting groups were removed upon TBAF treatment. Although the lipidic nature of squalene precluded crystallization of the intermediates, a satisfactory purity (≥ 98% by HPLC) was achieved after optimization of the chromatographic conditions for both Lab SQAd and Ind SQAd. NMR analysis of both batches yielded spectra consistent with SQAd (Supplementary Figure S2). Nanoparticles of both Lab SQAd and Ind SQAd were then formulated to evaluate the influence of industrial scale-up on NPs properties.

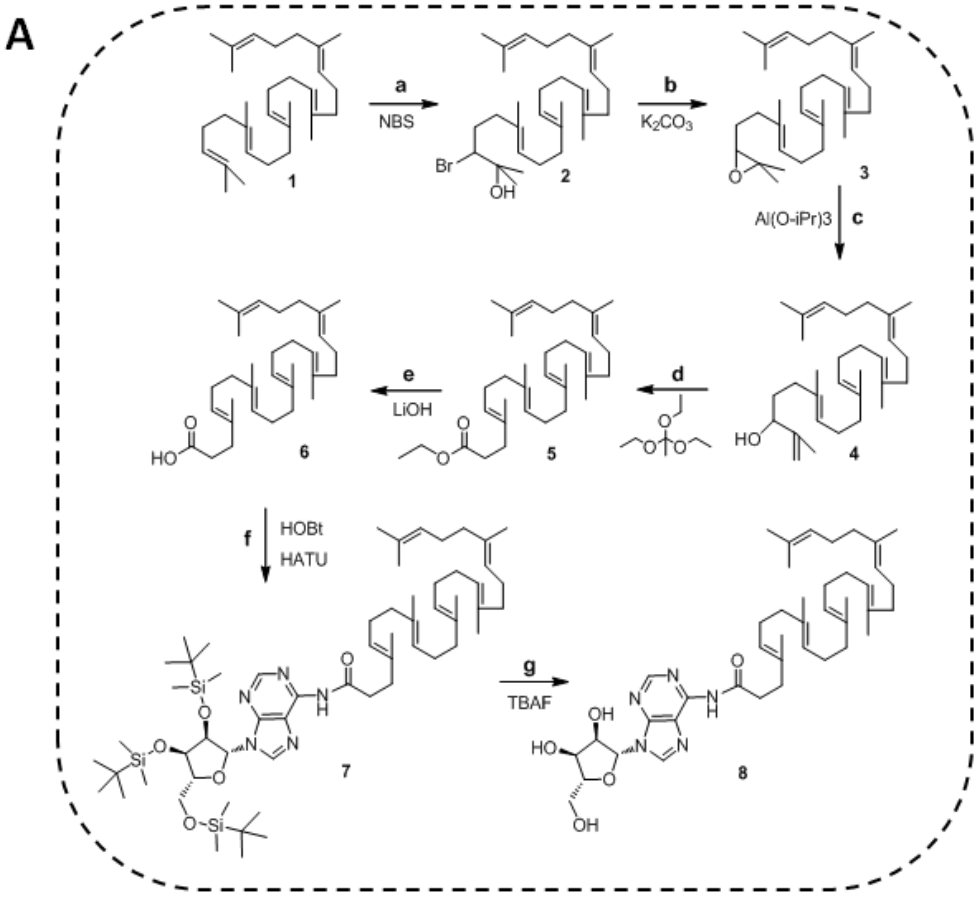

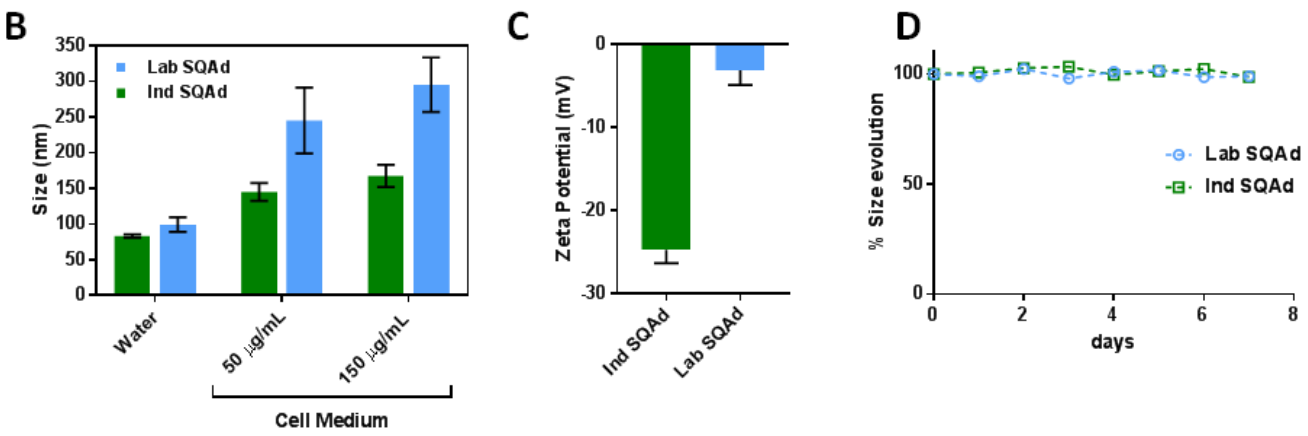

Fig. 1. A. Scheme of SQAd synthesis: a) Squalene and NBS in THF/H2O, 29%. b) 2 and K2CO3 in MeOH, 95%. c) 3, aluminium-isopropoxide in Toluene, reflux, 63%. d) 4, propionic acid in triethyl orthoacetate, reflux. e) 5, LiOH,H_2O in EtOH/THF, reflux, 65%. f) 6, HOBt, HATU and DIPEA in DCM, 45%. g) 7 and TBAF in THF, 55%. **B.** DLS measurement of NPs sizes for Lab SQAd and Ind SQAd batches. For measurements performed in cell medium, NPs were dispersed at a concentration of 50 µg/mL or 150 µg/mL in complete DMEM medium. **C.** Zeta-potential measurements of Lab SQAd and Ind SQAd. **D.** Stability of SQAd NPs in water determined by DLS monitoring of NP size ring opening reaction (c) followed by Claisen-Johnson rearrangement with triethylorthoacetate (d) [26]. After saponification, the obtained squalenyl acetic acid was coupled to 2',3',5'-trisilylated adenosine using HATU/HOBt as coupling agent with moderate yield. After extensive purification, the silyl protecting groups were removed upon TBAF treatment. Although the lipidic nature of squalene precluded crystallization of the intermediates, a satisfactory purity (≥ 98% by HPLC) was achieved after optimization of the chromatographic conditions for both Lab SQAd and Ind SQAd. NMR analysis of both batches yielded spectra consistent with SQAd (Supp. Fig. S2). Nanoparticles of both Lab SQAd and Ind SQAd were then formulated to evaluate the influence of industrial scale-up on NPs properties.

3.2.12. NP formulation and physico-chemical characterization

SQAd NPs were prepared as previously described[18] by nanoprecipitation of an ethanolic solution of SQAd in a 5% (w/v) aqueous dextrose solution. Once formulations of different SQAd batches were obtained, size and polydispersity index (PDI) of the NPs were measured by dynamic light scattering

(DLS) (Figure 1B). The measurements obtained showed substantial differences in the colloidal behavior of formulations originating from different SQAd batches. Indeed, small variation in the mean size were observed (83 nm / 99 nm for respectively Ind SQAd and Lab SQAd) while large differences in the mean zeta potential were measured (from -25mV to -5mV for respectively Ind SQAd and Lab SQAd) (figure 1C). Both formulations were stable for at least 7 days in water as measured by DLS data (Figure 1D), while in cell culture medium Ind SQAd NPs were found to be more stable than Lab SQAd NPs. This difference was most probably due to their stronger surface charge which inhibited NPs aggregation in a solution of high ionic strength such as cell medium. In addition, cryo-TEM imaging (Figure 2A-B) showed substantial differences concerning the NPs internal structure. Lab SQAd demonstrated apparent internal ordering while Ind SQAd produced NPs with less apparent structure. To further investigate this observation, the internal structure of SQAd NPs was studied by Small-Angle X-ray Scattering (SAXS) (Figure 2C-D). For Lab SQAd, the SAXS pattern displayed three Bragg reflections at q_0 = 0.091 $Å^{-1}$, q_1 = 0.158 $Å^{-1}$ ($q_0\sqrt{3}$) and q_2 = 0.182 $Å^{-1}$ ($2q_0$). These peaks indexed as the reflections of an inverse 2D hexagonal phase with lattice parameter a = 78.0 Å. For Ind SQAd, however, SAXS data showed only one smooth Bragg peak without high order reflections, in agreement with a lower ordering of the internal structure, as observed by cryoTEM. The low ordering of Ind SQAd NPs suggested that some constituents of the SQAd NPs batches may influence NPs colloidal behavior and warranted further studies to evaluate if these physico-chemical differences may impact the biological behavior of NPs.

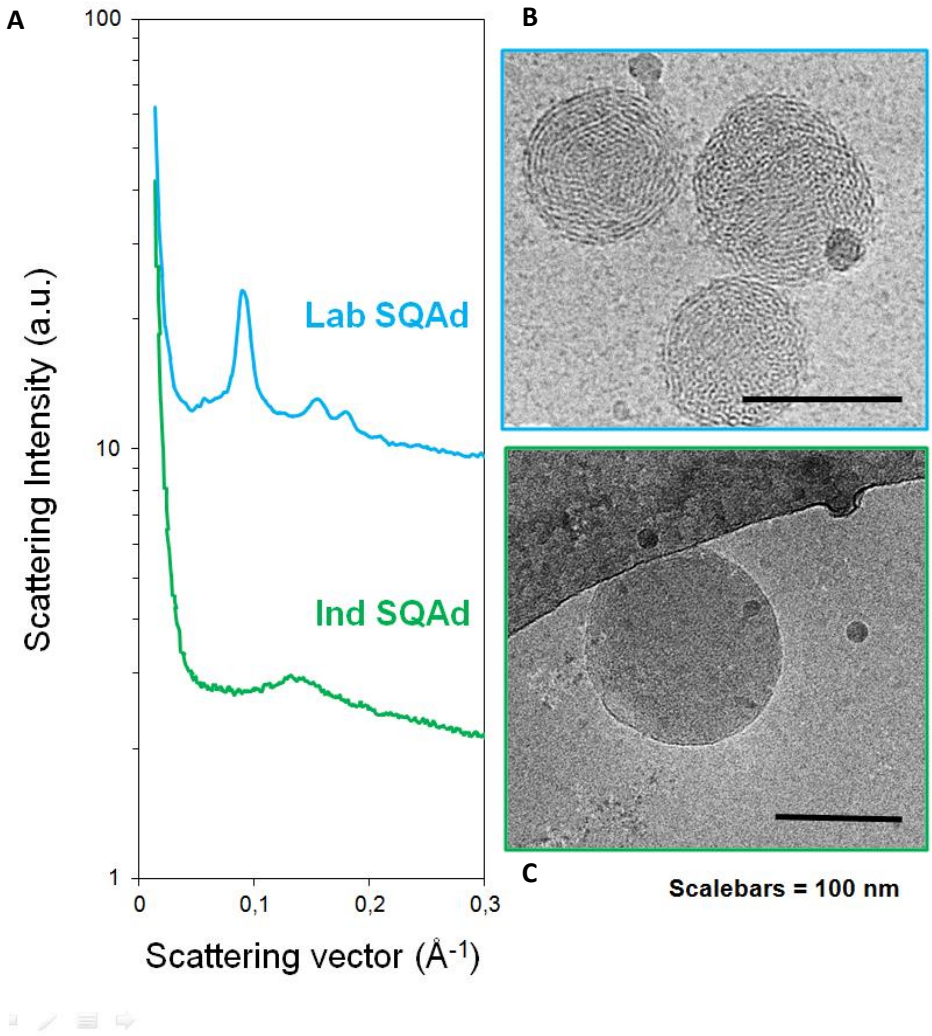

Fig. 2: A. Small-angle X-ray diffraction patterns NPs recorded at room temperature. **B.** Selected Cryo-TEM image of Lab SQAd NPs obtained by nanoprecipitation of an ethanolic solution in DXT 5%. **C.** Selected Cryo-TEM image of Ind SQAd NPs obtained by nanoprecipitation of an ethanolic solution in DXT 5%.

3.1.3. Cytotoxicity of Lab SQAd and Ind SQAd batches

In this study, HepG2, HUVEC, HL1 and MiaPaca cells lines were chosen as *in vitro* models of the influence of SQAd to account for cell subtype-specific variations. The cytotoxicity of different batches of SQAd NPs was determined after incubation with the various cell lines by performing an MTT assay (Figure 3). Ind SQAd batches were consistently found to be more toxic than lab SQAd NPs with IC_{50}

values in the 100 μM range while Lab SQAd did not induce a strong cytotoxicity even at concentrations of 200 μM. This tendency was confirmed on the four tested cell lines and with NPs incubation times ranging from 24 to 72 hours. Also, the presence of dextrose in the formulations did not to influence the cytotoxicity of SQAd NPs (Supplementary Figure S3).

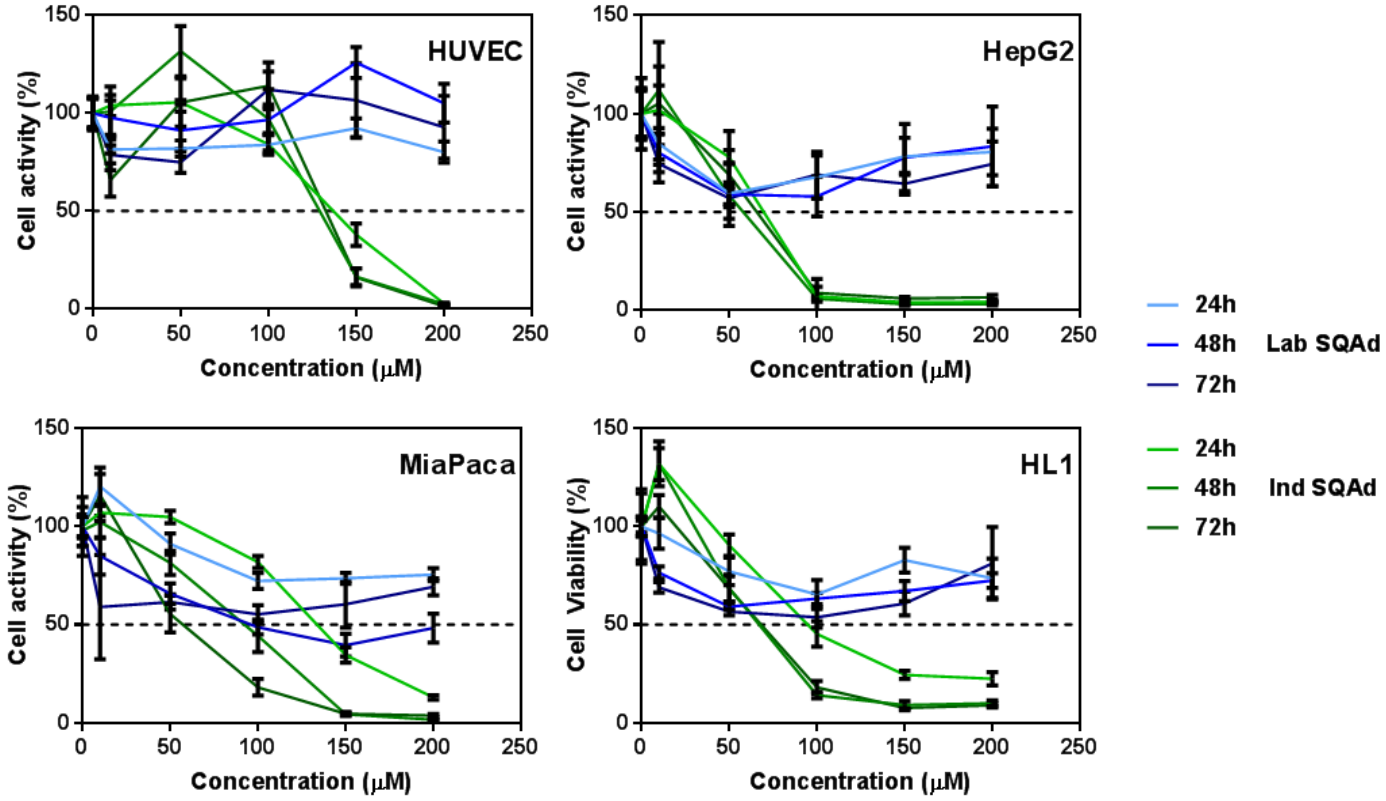

Fig.3: MTT assays of Lab SQAd and Ind SQAd on HUVEC, HepG2, MiaPaca and HL1 cell lines. Viability was expressed as % of viability of non-treated cells as measured by formazan dye absorbance at 570 nm. Concentrations ranging from 5 μM to 200 μM were studied over 24 h, 48 h and 72 h of incubation.

Squalene is an endogenous precursor of cholesterol which is non-toxic to cells. Once functionalized into squalenylacetic acid **6**, it has been shown to induce a moderate inhibition of cell proliferation in certain models with IC_{50} concentrations in the 180-200 μM ranges on HUVEC and MiaPaca cells[27]. Adenosine, on the other hand, has a more controversial effect on cell proliferation [28-30]. While it can

induce apoptosis and cell death in certain types of cardiomyocytes[31] and neutrophils[32], adenosine provides important cytoprotective functions in the heart and brain tissue during ischemia, hypoxia or ischemia reperfusion[33,34]. A number of studies have reported that cell specific purinergic receptors contribute to the dual effects of adenosine on cell viability[35-37]. SQAd has been shown not to be a direct agonist of these purinergic adenosine receptors but rather to act through accumulation of adenosine intracellularly[38]. In any case, these subtle cytotoxic and cytoprotective effects of adenosine can hardly explain the gross differences displayed in the cytotoxicity profiles of the different SQAd batches observed in this study.

3.1.4. Plasma protein adsorption

Current understanding of the nano-bio interfaces suggests that the protein corona (*ie* surface adsorbed proteins) formed on nanoparticles greatly influences their biological fate[39,40]. Consequently, plasma protein adsorption on Ind SQAd NPs and Lab SQAd NPs was evaluated after incubation in rat plasma for 1 h at 37 °C. NP-protein complexes were isolated from excess plasma, washed thoroughly, and the amount of adsorbed proteins was quantified for each formulation. Lab SQAd formulations afforded an average of 37.4 µg/mL (i.e. 93.5 µg/mg NPs) adsorbed proteins, while Ind SQAd afforded an average of only 12.8 µg/mL (i.e. 32 µg/mg NPs) adsorbed proteins. These values refer to those proteins which strongly interacted with the nanoparticles surface, the so called “hard corona”, which essentially confer the NPs their biological identity. Although previous studies have shown that strongly negative NPs had a tendency to adsorb higher amount of proteins[41], the main driving force in protein-NP interactions is not simply electrostatic but revolves also around complex colloidal and biochemical interactions which characterize the NPs *in vivo*[42,43]. For instance, it is possible that the crystal lattice of the Lab SQAd nanoparticles allowed greater access and interaction with the small proteins of the plasma.

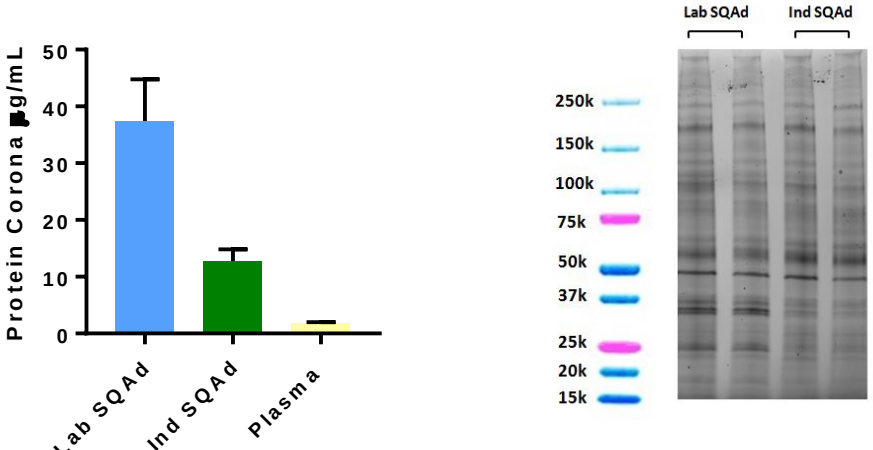

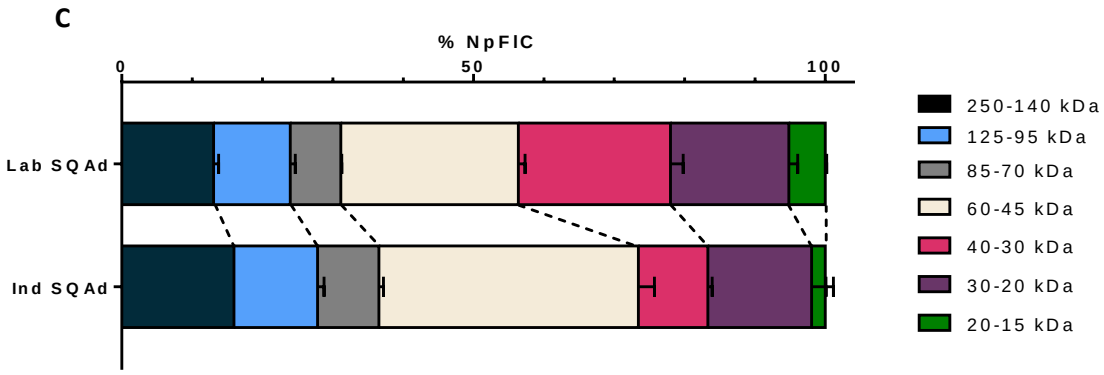

Figure 4: A. Concentration of protein corona isolated from different batches of SQAd NPs as measured by Pierce protein assay. For plasma control, the same procedure as for NPs corona evaluation was used but without the presence of nanoparticles. **B.** 1D-PAGE of duplicates of Lab SQAd and Ind SQAd protein corona samples. Molecular weight ladder was migrated with a pre-stained Biorad Precision Plus sample which is shown alongside the stain-free gel electrophoresis. **C.** Normalized Percentage of Fluorescence Count for proteins found in the hard corona of Lab SQAd and Ind SQAd nanoparticles. Proteins were grouped following molecular weight expressed in kDa.

To better identify the influence of the industrial scale-up on the nature of the adsorbed proteins at the surface of the NPs, stain-free 1D-PAGE was performed on the hard corona isolated from NPs of both Lab SQAd and Ind SQAd batches (Figure 4B). 1D-PAGE resolves the corona proteins according to their molecular weight and afforded a basic evaluation of the different fractions of protein adsorbed to the NPs and their relative amounts.

The relative abundance of each protein fraction on the surface of the nanoparticles was evaluated by Normalized Percentage of Fluorescence Count (%NpFlC, equivalent to the fraction of total fluorescence for all proteins found in the corona). The protein corona compositions shown in Figure 4C varied in subtle ways between the two SQAd batches. Mainly, low molecular weight protein fractions appeared to be significantly reduced in Ind SQAd and could account for the smaller quantities of protein corona found on Ind SQAd NPs. On the contrary, proteins of larger molecular weight (above 60 kDa) were

found to be present consistently among the tested nanoparticles samples (lane profiles can be found in Supplementary Figures S7-8). While the determinants of corona composition are often underappreciated and hardly characterized, they are critical in determining the subsequent fate and effects of NPs in both *in vitro* and *in vivo* situations. Studies have shown that variations of less than 10 % in the makeup of a NP's protein corona could result in an alteration of the pharmacokinetic profiles and biodistribution[40].

3.2. Identification and characterization of impurities

3.2.1. Chromatography studies

Our previous physico-chemical and *in-vitro* studies seemed to point to the presence of formerly undetected impurities, especially in the Ind SQAd batches. As such, a more sensitive HPLC-MS approach of the different SQAd samples was carried out in order to identify and characterize eventual impurities responsible for batch-to-batch discrepancies. The results, shown in Fig. 5, indicate that other than SQAd (peaks 3 and 4) a small quantity of detectable impurity phase, from now on named Ph1, corresponding to a mass of elution peaks around 20.8 min (peaks 1,2 and 5), was present in Ind SQAd batches. UV integration at 270 nm showed Ph1 peaks present at 1–2% in Ind SQAd and hardly detectable (< 0.5%) in Lab SQAd. ES-MS data showed Ph1 as being composed of a mixture of SQAd analogs with major components having measured masses of 734.48 g/mol and 750.47 g/mol. Two minor impurities were also found in shoulder 6 for which a MS study can be found in Supp. Fig. S6.

A

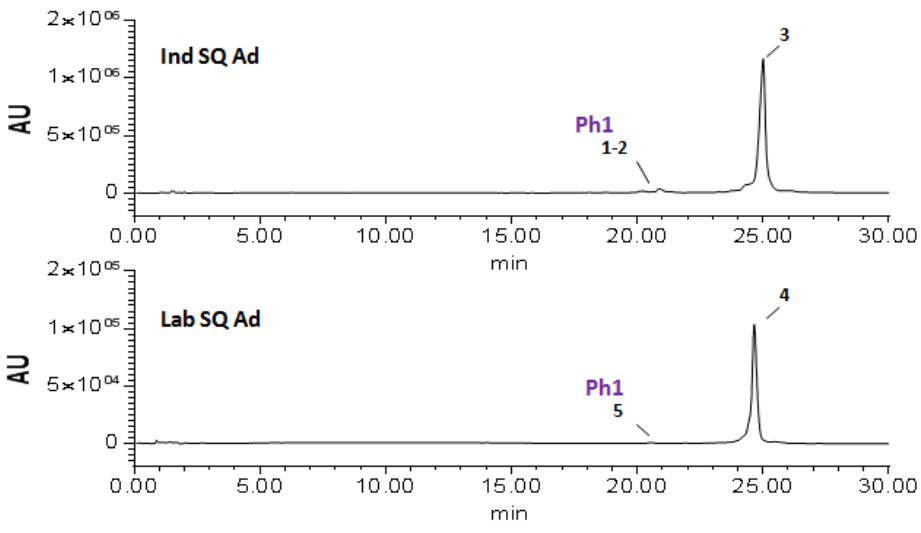

Table 1

Peak no	Identification	t_R (min)	Proposal ions	Measured mass (m/z)	Elemental composition	UV Integration (%)
1	SQAd OH_2	20.22	$[M-H]^+$	750.47	$C_{42}H_{63}N_5O_7$	0.5
2	SQAd OH	20.87	$[M-H]^+$	734.48	$C_{42}H_{63}N_5O_6$	1.5
3	SQAd	25.00	$[M-H]^+$	718.49	$C_{42}H_{63}N_5O_5$	98
4	SQAd	24.73	$[M-H]^+$	718.49	$C_{42}H_{63}N_5O_5$	99.5
5	SQAd OH	20.52	$[M-H]^+$	734.48	$C_{42}H_{63}N_5O_6$	0.5

Figure 5: UV-HPLC spectra of Ind SQAd and Lab SQAd. SQAd bioconjugates were dissolved in EtOH and injected into the HPLC system. UV spectra was recorded at 268 nm, corresponding to the maximum absorption peak of SQAd. At the end of the HPLC system, ES mass spectrometry was performed with results reported in Figure 5B**.**

To elucidate this further, a collision induced dissociation (CID) MS^n study of these two compounds was carried out (Table 2 and Supp. Figs. S7-S9). CID of SQAd in the conditions used for this study usually yields a single major product ion with *m/z* = 586.44, corresponding to the fragmentation of a ribose residue from the adenosine moiety. When CID was carried out on Ph1, it showed that both compounds with *m/z* = 734.48 and *m/z* = 750.47 first demonstrated the usual pathway of parent ion fragmentation observed with secondary allylic alcohols, corresponding to a β-elimination of the hydroxyl group, followed by the expected product ions induced by SQAd ion fragmentation. Of note, chromatograms obtained from the high resolution HPLC-ESI-MS^n study additionally showed that slightly different elution peaks corresponded to compounds having identical molecular masses (Figure 6C). For single –OH substituted compounds, we found five elution peaks corresponding to the five possible substitution products over the available isoprenyl subunits, while double –OH substituted compounds gave 10 elution peaks corresponding to the combination of two substitutions out of a set of five available isoprenyl subunits.

Table 2

Compound	Parent ion (m/z)	MS^1 Product (m/z)	MS^2 Product (m/z)
SQAd	718.49	586.44	
SQAd OH	734.48	716.47	
		602.44	
	602.44		584.43
SQAd OH_2	750.47	732.47	
		714.47	
		618.44	
	618.44		600.43
			584.43

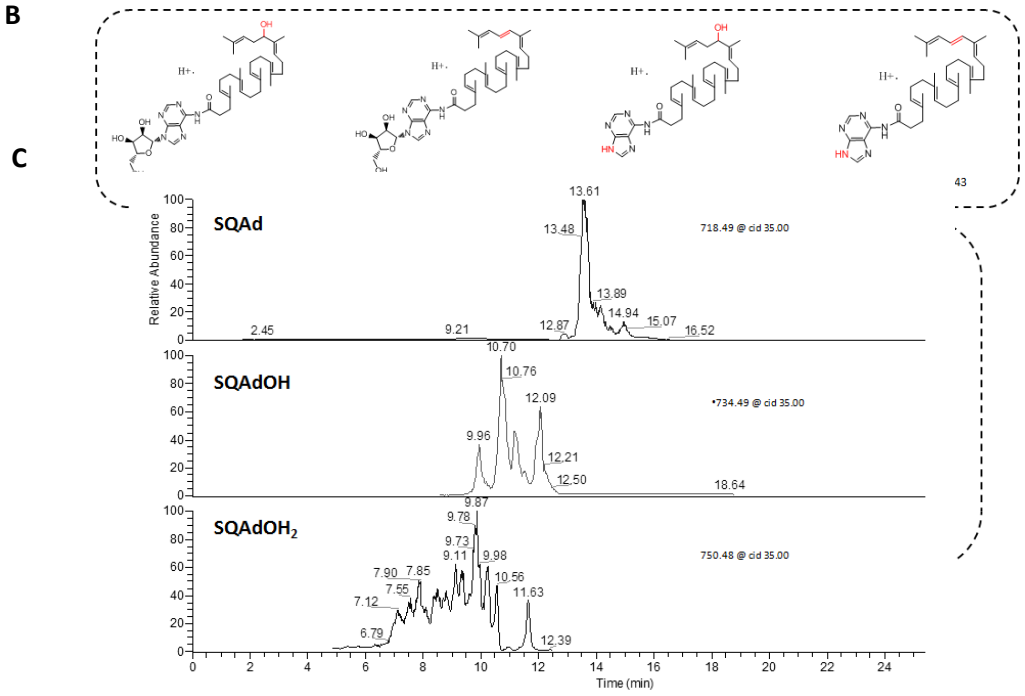

Figure 6: A. Collision induced dissociation of the different SQAd compounds detected by MS^n. **B.** Presumptive structures for the detected SQAd analogs and their collision-induced product ions are shown. Upper box shows product ions for single –OH substituted SQAd analogs, lower box corresponds to double –OH substituted products. Exact masses were calculated with the ChemDraw software and fitted the experimental data. **C.** Chromatograms of the different SQAd analogs obtained during HPLC-ESI-MS^n.

This indicated that the SQAd analogs most probably existed as a mixture of isomers in Ph1, suggesting that the oxidative side-reaction which led to the additional hydroxyl groups occurred unselectively over all five isoprenyl subunits. Although, in the absence of an exact structural determination, the mechanism of formation of these minor byproducts remains speculative, it can be suggested that they result from the ring-opening reaction with aluminum isopropoxide of internal epoxides produced by over oxidation with NBS. Previous studies have shown that the main side product in the van Tamelen

procedure is the ω,ω-bis-bromohydrine[44,45]. During the purification process, using chromatography on silica gel, only the main side product corresponding to the ω,ω-bis-bromohydrine could be separated, while minor less polar internal bromohydrines are much more difficult to eliminate and could remain with the main product. Once formed, these highly hindered allylic alcohols would not act as substrates in the Claisen-Johnson transposition and thus would remain as minor components in the bulk main product.

a) Cytotoxicity of hydroxylated SQAd impurities

To elucidate the impact of Ph1 impurities on the observed batch-to-batch discrepancies in NPs properties, a preparative HPLC separation (HPLC-Prep) was performed to isolate Ph1 from SQAd. Practically, two series of experiments were performed (Figure 7). First, Ph1 only NPs were prepared and tested as such for their cytotoxicity and physicochemical properties. When prepared by nanoprecipitation, Ph1 yielded stable NPs and DLS data showed a strongly negative zeta potential of -35 mV and sizes of ca. 100 nm. Further studies focused on the biological effects of Ph1 NPs which were found to be dramatically cytotoxic (IC_{50} values around 5 μM) comparatively to purified SQAd which barely induced cytotoxicity in the tested concentration ranges. Later, a series of additional experiments were performed in which pure SQAd was spiked with increasing concentrations of Ph1 (from 0.1 % w/w to 10 % w/w). Remarkably, the amount of Ph 1 was proportionally linked to cytotoxicity in SQAd nanoformulations (Figure 7F).

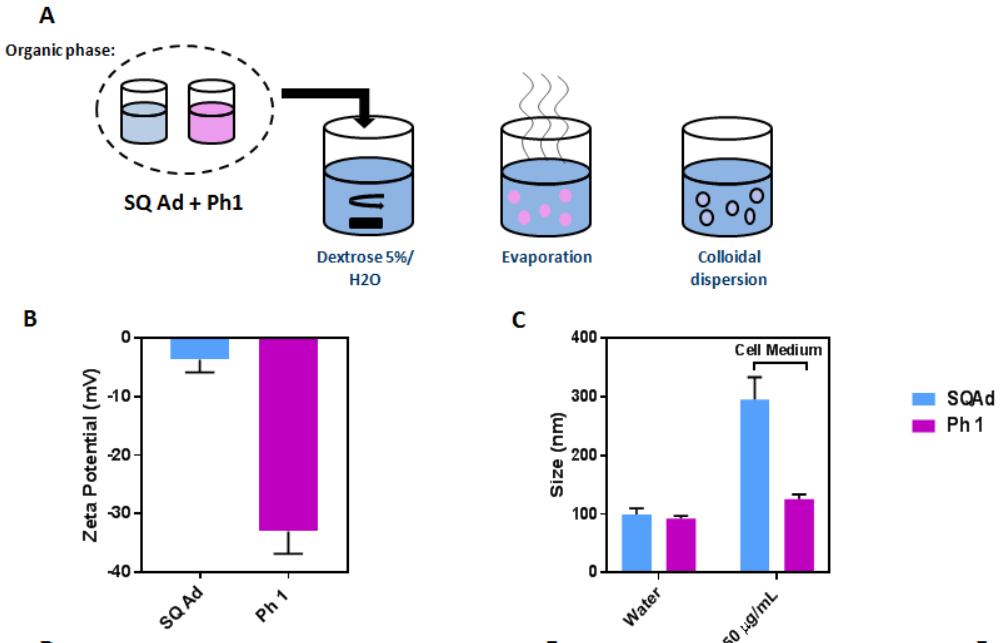

Figure 7: A. Representative scheme of spiking experiments, where isolated Ph1 and SQAd eluates were combined in varying ratios. **B.** Zeta-potential measurements of SQAd and Ph1 NPs. **C.** DLS size measurement of SQAd and Ph1 NPs. For measurements performed in cell medium, NPs were dispersed at 150 μg/mL in complete DMEM medium. **D-E.** MTT assays of SQAd and Ph1 NPs on MCEC and HepG2 cell lines. Cell viability was measured as % viability of non treated cells. **F.** Cell viability after 24 hours incubation with 100 μM of SQAd eluate NPs or NPs of SQAd spiked with 0.1%-10% w/w of Ph1.

These experiments confirmed that the Ph1 impurity, even when present in small quantity, was responsible for both the biological and physicochemical alteration of SQAd NPs properties. It is not surprising that Ph1 forms a stable colloidal phase when nanoformulated due to the strongly negative zeta potential it imparts to the resulting nanoparticles. We postulated that the observed cytotoxic effect of Ph1 is likely due to aberrant squalene chains altering the cell membrane integrity [46]. Indeed, squalene strongly interacts with lipid bilayers because of its structural similarity with cholesterol and through binding to LDL receptors on the cell surface [21,47,48]. Additionally, it is also possible that hydroxylated SQAd analogs can participate in oxidative stress signaling through their similitude with lipid peroxidation by-products.

Ultimately, nanoparticle-based delivery systems are unique structures capable of accumulating bioactive molecules inside tissues and cells. This makes them a class of materials that is especially sensitive to the presence of residual manufacturing components or variations in purity from batch to batch [49-51]. This has often lead to misjudgments concerning NP toxicities and poor reproducibility of results[52,53]. Here, even though special precautions were taken in using biocompatible reagents and formulation strategies, scaling-up the manufacturing process resulted in varying quantities of analogs of the lipid carrier chain which in turn were responsible for an unexpected cytotoxicity of SQAd NPs. These findings highlight the complexity of nanotechnology and the escalating level of expertise required to successfully generate safe and efficient nanomedicines. Not only does it require a thorough understanding of the chemistry and biocompatibility of compounds used for the initial formulation of the nanoparticles, but also full comprehension of the synthesis process and its implications on the aforementioned properties. In a context where the reproducibility of nanoformulations is put into question[54] and numerous generics of approved nanoformulated drugs are set to enter the market in the coming years[55], special care and regulatory oversight over these issues is of outmost importance.

Conclusions:

In this study, we show that the scale-up of the bromohydrine synthetic pathway to SQAd can alter the impurity profile of the squalene bioconjugate which results in critical variations in SQAd NPs properties. Here, close analogs of the carrier lipid chain were found to be highly cytotoxic and strenuous to separate from SQAd bulk by conventional chromatographic methods. Surprisingly, these minor impurities had a strong impact on the colloidal properties, internal structure and biological properties of SQAd NPS. Identifying these issues was crucial in finally obtaining batches of SQAd that yield nanoparticles with consistent properties, which has now been achieved by the industrial partner.

Failure to properly characterize a material has afflicted the nanotechnology field for many years, regularly leading to misjudgments about the properties of nanoparticles. The matter is often made worse in the case of nanocarriers because of the inherent polydispersity of their physico-chemical properties as well as their plural chemical identity. Identifying which parameters are most important for establishing the therapeutic and biological equivalence of two nanoparticle formulations is therefore important. As the field matures and a growing number of products seek regulatory approval, an especially careful approach in terms of toxicity and pharmaceutical development should be adopted in the maturation process of these innovative materials. Ultimately, understanding and solving these issues is a crucial part of the advancement of nanomedicines, and one which cannot be left for the industry to deal with alone.

***Abbreviations**:* SQAd, Squalene-Adenosine; NBS, N-Bromosuccinimide; HOBt, 1- hydroxybenzotriazole hydrate; HATU, 2-(1H-7-azabenzotriazol-1-yl)-1,1,3,3-tetramethyluronium hexafluorophosphate; DIIPEA, Diisopropylethylamine; MTT, 3-(4,5-dimethylthiazol-2-yl)-2,5-diphenyltetrazolium bromide; DMEM, Dulbecco's Modifidied Eagle's Medium; DXT, Dextrose; THF, Tetrahydrofurane; NMR, Nuclear Magnetic Resonance; MTBE, Methyl *tert*-butyl ether; NPs, Nanoparticles; DLS, Dynamic Light Scattering; FBS, Fetal Bovine Serum; PBS, Phosphate-buffered saline; ES-MS, Electrospray Mass Spectrometry; TEM, Transmission Electron Microscopy; ATP, Adenosine tri-phosphate; SDS, Sodium dodecyl phospage; PAGE, Polyacrylamide gel electrophoresis

Funding: The authors gratefully acknowledge the financial support from the 7th EuroNanoMed-II call for proposals, project NanoHeart n°ANR-16-ENM2-0005-01. This work was further supported by la Fondation pour la Recherche Médicale (FRM) grant number ECO20160736101. Cryo-TEM observations were made thanks to “Investissements d’Avenir” LabEx PALM (ANR-10-LABX-0039-PALM).

Acknowledgments: The authors wish to thank Karine Leblanc from the BioCIS platform for her expert technical advice on running and performing chromatography experiments as well as Audrey Solgadi from UMS-IPSIT SAMM platform for her help in designing and performing the MS^n experiments as well as helpful corrections in the manuscript. Jéril Degrouard is thanked for his technical help and discussions relating to cryo-TEM images.

Legends:

Figure 1: A. Scheme of SQAd synthesis : a) Squalene and NBS in THF/H2O, 29% b) 2 and K_2CO_3 in MeOH, 95% c) 3, aluminium-isopropoxide in Toluene, reflux, 63% d) 4, propionic acid in triethyl orthoacetate, reflux e) 5, LiOH,H_2O in EtOH/THF, reflux, 65% f) 6, HOBt, HATU and DIPEA in DCM, 45% f) 7 and TBAF in THF, 55%. **B.** DLS measurement of NPs sizes for Lab SQAd and Ind SQAd batches. For measurements performed in cell medium, NPs were dispersed at a concentration of 50 μg/mL or 150 μg/mL in complete DMEM medium. **C.** Zeta-potential measurements of Lab SQAd and Ind SQAd. **D.** Stability of SQAd NPs followed by DLS size measurement.

Figure 2: A. Small-angle X-ray diffraction patterns NPs recorded at room temperature. **B.** Selected Cryo-TEM image of Lab SQAd NPs obtained by nanoprecipitation of an ethanolic solution in DXT 5%. **C.** Selected Cryo-TEM image of Ind SQAd NPs obtained by nanoprecipitation of an ethanolic solution in DXT 5%.

Figure 3: MTT assays of Lab SQAd and Ind SQAd on HUVEC, HepG2, MiaPaca and HL1 cell lines. Viability was measured as % of viability of non treated cells as measured by formazan dye absorbance at 570 nm. Concentrations ranging from 5 μM to 200 μM were studied.

Figure 4: A. Concentration of protein corona isolated from different batches of SQAd NPs as measured by Pierce protein assay. For plasma control, the same procedure as for NPs corona evaluation was used but without the presence of nanoparticles. **B.** 1D-PAGE of duplicates of Lab SQAd and Ind SQAd protein corona samples. Molecular weight ladder was migrated with a pre-stained Biorad Precision Plus sample which is shown alongside the stain-free gel electrophoresis. **C.** Normalized Percentage of Fluorescence Count for proteins found in the hard corona of Lab SQAd and Ind SQAd nanoparticles. Proteins were grouped following molecular weight expressed in kDa.

Figure 5: UV-HPLC spectra of Ind SQAd and Lab SQAd. SQAd bioconjugates were dissolved in EtOH and injected into the HPLC system. UV spectra was recorded at 268 nm, corresponding to the maximum absorption peak of SQAd. At the end of the HPLC system, ES mass spectrometry was performed with results reported in Figure 5B**.**

Figure 6: A. Collision induced dissociation of the different SQAd compounds detected by MS^n. **B.** Presumptive structures for the detected SQAd analogs and their collision induced product ions are shown. Upper box shows product ions for single –OH substituted SQAd analogs, lower box corresponds to double –OH substituted products. Exact masses were calculated with the ChemDraw software and fitted to experimental data. **C.** Chromatograms of the different SQAd analogs obtained during HPLC-ESI-MS^n.

Figure 7: A. Representative scheme of spiking experiments, where isolated Ph1 and SQAd eluates were combined in varying ratios. **B.** Zeta-potential measurements of SQAd and Ph1 NPs. **C.** DLS size measurement of SQAd and Ph1 NPs. For measurements performed in cell medium, NPs were dispersed at 150 μg/mL in complete DMEM medium. **D-E.** MTT assays of SQAd and Ph1 NPs on MCEC and HepG2 cell lines. Cell viability was measured as % viability of non treated cells. **F.** Cell viability after 24 hours incubation with 100 μM of SQAd eluate NPs or NPs of SQAd spiked with 0.1%-10% w/w of Ph1.

Abbreviations:

SQAd : Squalene-Adenosine

NBS: N-Bromosuccinimide

HOBt: 1- hydroxybenzotriazole hydrate

HATU: 2-(1H-7-azabenzotriazol-1-yl)-1,1,3,3-tetramethyluronium hexafluorophosphate

DIIPEA: Diisopropylethylamine

Et3N: Triethylamine

MTT: 3-(4,5-dimethylthiazol-2-yl)-2,5-diphenyltetrazolium bromide

DMEM: Dulbecco's Modifidied Eagle's Medium

DXT: Dextrose

THF: Tetrahydrofurane

MeOH: Methanol

K_2CO_3: Potassium Carbonate

AcOEt: Ethyl Acetate

NMR: Nuclear Magnetic Resonance

$CDCl_3$: Chloroform-d

$MgSO_4$: Magnesium Sulfate

MTBE: Methyl *tert*-butyl ether

NPs: Nanoparticles

DLS: Dynamic Light Scattering

KCl: Potassium Chloride

FBS: Fetal Bovine Serum

PBS: Phosphate-buffered saline

ES-MS: Electrospray Mass Spectrometry

TEM: Transmission Electron Microscopy

ATP: Adenosine tri-phosphate

SDS: Sodium dodecyl phospage

PAGE: Polyacrylamide gel electrophoresis

1. Mura S, Nicolas J, Couvreur P (2013) Stimuli-responsive nanocarriers for drug delivery. Nature materials 12: 991.
2. Kakkar A, Traverso G, Farokhzad OC, Weissleder R, Langer R (2017) Evolution of macromolecular complexity in drug delivery systems. Nature Reviews Chemistry 1: 0063.
3. Venditto VJ, Szoka Jr FC (2013) Cancer nanomedicines: so many papers and so few drugs! Advanced drug delivery reviews 65: 80-88.
4. Coty J-B, Vauthier C (2018) Characterization of nanomedicines: A reflection on a field under construction needed for clinical translation success. Journal of controlled release.
5. Seiffert J, Hussain F, Wiegman C, Li F, Bey L, et al. (2015) Pulmonary toxicity of instilled silver nanoparticles: influence of size, coating and rat strain. PloS one 10: e0119726.
6. Wang H-X, Zuo Z-Q, Du J-Z, Wang Y-C, Sun R, et al. (2016) Surface charge critically affects tumor penetration and therapeutic efficacy of cancer nanomedicines. Nano Today 11: 133-144.
7. Qin S-Y, Cheng Y-J, Jiang Z-W, Ma Y-H, Zhang A-Q (2018) Morphology control of self-deliverable nanodrug with enhanced anticancer efficiency. Colloids and Surfaces B: Biointerfaces 165: 345-354.
8. Stern ST, Hall JB, Lee LY, Wood LJ, Paciotti GF, et al. (2010) Translational considerations for cancer nanomedicine. Journal of Controlled Release 146: 164-174.
9. Bertrand N, Grenier P, Mahmoudi M, Lima EM, Appel EA, et al. (2017) Mechanistic understanding of in vivo protein corona formation on polymeric nanoparticles and impact on pharmacokinetics. Nature communications 8: 777.
10. Mamidi RN, Weng S, Stellar S, Wang C, Yu N, et al. (2010) Pharmacokinetics, efficacy and toxicity of different pegylated liposomal doxorubicin formulations in preclinical models: is a conventional bioequivalence approach sufficient to ensure therapeutic equivalence of pegylated liposomal doxorubicin products? Cancer chemotherapy and pharmacology 66: 1173-1184.
11. Ragelle H, Danhier F, Préat V, Langer R, Anderson DG (2017) Nanoparticle-based drug delivery systems: a commercial and regulatory outlook as the field matures. Expert opinion on drug delivery 14: 851-864.
12. Crist RM, Grossman JH, Patri AK, Stern ST, Dobrovolskaia MA, et al. (2012) Common pitfalls in nanotechnology: lessons learned from NCI's Nanotechnology Characterization Laboratory. Integrative Biology 5: 66-73.
13. Desmaële D, Gref R, Couvreur P (2012) Squalenoylation: a generic platform for nanoparticular drug delivery. Journal of controlled release 161: 609-618.
14. Lepeltier E, Loretz B, Desmaële D, Zapp J, Herrmann J, et al. (2015) Squalenoylation of chitosan: a platform for drug delivery? Biomacromolecules 16: 2930-2939.
15. Couvreur P (2016) Squalenoylation: a novel technology for anticancer and antibiotic drugs with enhanced activity. Nanosciences and Nanotechnology: Springer. pp. 253-272.
16. Reddy LH, Khouri H, Paci A, Deroussent A, Ferreira H, et al. (2008) Squalenoylation favourably modifies the in vivo pharmacokinetics and biodistribution of gemcitabine in mice. Drug Metabolism and Disposition.
17. Maksimenko A, Mougin J, Mura S, Sliwinski E, Lepeltier E, et al. (2013) Polyisoprenoyl gemcitabine conjugates self assemble as nanoparticles, useful for cancer therapy. Cancer letters 334: 346-353.
18. Gaudin A, Yemisci M, Eroglu H, Lepetre-Mouelhi S, Turkoglu OF, et al. (2014) Squalenoyl adenosine nanoparticles provide neuroprotection after stroke and spinal cord injury. Nature nanotechnology 9: 1054.
19. Feng J, Lepetre-Mouelhi S, Gautier A, Mura S, Cailleau C, et al. (2019) A new painkiller nanomedicine to bypass the blood-brain barrier and the use of morphine. Science Advances 5: eaau5148.

20. Gaudin A, Lepetre-Mouelhi S, Mougin J, Parrod M, Pieters G, et al. (2015) Pharmacokinetics, biodistribution and metabolism of squalenoyl adenosine nanoparticles in mice using dual radio-labeling and radio-HPLC analysis. Journal of Controlled Release 212: 50-58.
21. Gaudin A, Tagit O, Sobot D, Lepetre-Mouelhi S, Mougin J, et al. (2015) Transport mechanisms of squalenoyl-adenosine nanoparticles across the blood–brain barrier. Chemistry of Materials 27: 3636-3647.
22. Laemmli UK (1970) Cleavage of structural proteins during the assembly of the head of bacteriophage T4. nature 227: 680.
23. Van Tamelen E, Curphey T (1962) The selective in vitro oxidation of the terminal double bonds in squalene. Tetrahedron Letters 3: 121-124.
24. Ceruti M, Viola F, Dosio F, Cattel L, Bouvier-Navé P, et al. (1988) Stereospecific synthesis of squalenoid epoxide vinyl ethers as inhibitors of 2, 3-oxidosqualene cyclase. Journal of the Chemical Society, Perkin Transactions 1: 461-469.
25. Abad JL, Casas J, Sanchez-Baeza F, Messeguer A (1993) Dioxidosqualenes: characterization and activity as inhibitors of 2, 3-oxidosqualene-lanosterol cyclase. The Journal of Organic Chemistry 58: 3991-3997.
26. Johnson WS, Werthemann L, Bartlett WR, Brocksom TJ, Li T-T, et al. (1970) Simple stereoselective version of the Claisen rearrangement leading to trans-trisubstituted olefinic bonds. Synthesis of squalene. Journal of the American Chemical Society 92: 741-743.
27. Buchy E, Valetti S, Mura S, Mougin J, Troufflard C, et al. (2015) Synthesis and Cytotoxic Activity of Self-Assembling Squalene Conjugates of 3-[(Pyrrol-2-yl) methylidene]-2, 3-dihydro-1H-indol-2-one Anticancer Agents. European Journal of Organic Chemistry 2015: 202-212.
28. Schrier SM, van Tilburg EW, van der Meulen H, Ijzerman AP, Mulder GJ, et al. (2001) Extracellular adenosine-induced apoptosis in mouse neuroblastoma cells studies on involvement of adenosine receptors and adenosine uptake1. Biochemical pharmacology 61: 417-425.
29. Ethier MF, Chander V, Dobson Jr JG (1993) Adenosine stimulates proliferation of human endothelial cells in culture. American Journal of Physiology-Heart and Circulatory Physiology 265: H131-H138.
30. Fishman P, Bar-Yehuda S, Vagman L (1998) Adenosine and other low molecular weight factors released by muscle cells inhibit tumor cell growth. Cancer research 58: 3181-3187.
31. Shneyvays V, Jacobson K, Li A, Nawrath H, Zinman T, et al. (2000) Induction of apoptosis in rat cardiocytes by A3 adenosine receptor activation and its suppression by isoproterenol. Experimental cell research 257: 111-126.
32. Kohno Y, Sei Y, Koshiba M, Kim HO, Jacobson KA (1996) Induction of Apoptosis in HL-60 Human Promyelocytic Leukemia Cells by Adenosine A3Receptor Agonists. Biochemical and biophysical research communications 219: 904-910.
33. Bès S, Ponsard B, El Asri M, Tissier C, Vandroux D, et al. (2002) Assessment of the cytoprotective role of adenosine in an in vitro cellular model of myocardial ischemia. European journal of pharmacology 452: 145-154.
34. Ramkumar V, Hallam DM, Nie Z (2001) Adenosine, oxidative stress and cytoprotection. The Japanese Journal of Pharmacology 86: 265-274.
35. Barankiewicz J, Danks AM, Abushanab E, Makings L, Wiemann T, et al. (1997) Regulation of adenosine concentration and cytoprotective effects of novel reversible adenosine deaminase inhibitors. Journal of Pharmacology and Experimental Therapeutics 283: 1230-1238.
36. Jacobson KA (1998) Adenosine A3 receptors: novel ligands and paradoxical effects. Trends in pharmacological sciences 19: 184-191.
37. Imura T, Shimohama S (2000) Opposing effects of adenosine on the survival of glial cells exposed to chemical ischemia. Journal of neuroscience research 62: 539-546.
38. Rouquette M, Lepetre-Mouelhi S, Dufrancais O, Yang X, Mougin J, et al. (2019) Squalene-adenosine nanoparticles: ligands of adenosine receptors or adenosine prodrug? The Journal of pharmacology and experimental therapeutics.

39. Monopoli MP, Åberg C, Salvati A, Dawson KA (2012) Biomolecular coronas provide the biological identity of nanosized materials. Nature nanotechnology 7: 779.
40. Grenier P, de Oliveira Viana IM, Lima EM, Bertrand N (2018) Anti-polyethylene glycol antibodies alter the protein corona deposited on nanoparticles and the physiological pathways regulating their fate in vivo. Journal of controlled release 287: 121-131.
41. Walkey CD, Olsen JB, Song F, Liu R, Guo H, et al. (2014) Protein corona fingerprinting predicts the cellular interaction of gold and silver nanoparticles. ACS nano 8: 2439-2455.
42. Bigdeli A, Palchetti S, Pozzi D, Hormozi-Nezhad MR, Baldelli Bombelli F, et al. (2016) Exploring cellular interactions of liposomes using protein corona fingerprints and physicochemical properties. ACS nano 10: 3723-3737.
43. Liu R, Jiang W, Walkey CD, Chan WC, Cohen Y (2015) Prediction of nanoparticles-cell association based on corona proteins and physicochemical properties. Nanoscale 7: 9664-9675.
44. Hauptfleisch R, Franck B (1997) Stereoselective syntheses of 1, 24-dihydroxy squalene 2, 3; 22, 23-dioxides by double sharpless epoxidation. Tetrahedron letters 38: 383-386.
45. Hoshino T, Nakano S-i, Kondo T, Sato T, Miyoshi A (2004) Squalene–hopene cyclase: final deprotonation reaction, conformational analysis for the cyclization of (3 R, S)-2, 3-oxidosqualene and further evidence for the requirement of an isopropylidene moiety both for initiation of the polycyclization cascade and for the formation of the 5-membered E-ring. Organic & biomolecular chemistry 2: 1456-1470.
46. Mura S, Zouhiri F, Lerondel S, Maksimenko A, Mougin J, et al. (2013) Novel isoprenoyl nanoassembled prodrug for paclitaxel delivery. Bioconjugate chemistry 24: 1840-1849.
47. Peramo A, Mura S, Yesylevskyy SO, Cardey B, Sobot D, et al. (2018) Squalene versus cholesterol: Which is the best nanocarrier for the delivery to cells of the anticancer drug gemcitabine? Comptes Rendus Chimie.
48. Sobot D, Mura S, Yesylevskyy SO, Dalbin L, Cayre F, et al. (2017) Conjugation of squalene to gemcitabine as unique approach exploiting endogenous lipoproteins for drug delivery. Nature Communications 8: 15678.
49. Leonov AP, Zheng J, Clogston JD, Stern ST, Patri AK, et al. (2008) Detoxification of gold nanorods by treatment with polystyrenesulfonate. ACS nano 2: 2481-2488.
50. Liu J, Sonshine DA, Shervani S, Hurt RH (2010) Controlled release of biologically active silver from nanosilver surfaces. ACS nano 4: 6903-6913.
51. Zhu S, Oberdörster E, Haasch ML (2006) Toxicity of an engineered nanoparticle (fullerene, C60) in two aquatic species, Daphnia and fathead minnow. Marine Environmental Research 62: S5-S9.
52. Cortesi R, Esposito E, Menegatti E, Gambari R, Nastruzzi C (1996) Effect of cationic liposome composition on in vitro cytotoxicity and protective effect on carried DNA. International Journal of Pharmaceutics 139: 69-78.
53. Oberdörster E (2004) Manufactured nanomaterials (fullerenes, C60) induce oxidative stress in the brain of juvenile largemouth bass. Environmental health perspectives 112: 1058.
54. Leroux JC (2017) Drug Delivery: Too Much Complexity, Not Enough Reproducibility? Angewandte Chemie International Edition 56: 15170-15171.
55. Davenport M (2014) Closing the gap for generic nanomedicines. Chemical Engineering News 92: 10-13.